Viscous Fingering and Interfacial Instability Growth for Power-Law Fluids in Hele-Shaw Cells

Yao Zhang[1], Knut Erik Teigen Giljarhus[2], Hans Joakim Skadsem[1]

[1] Department of Energy and Petroleum Engineering, University of Stavanger, NO-4068 Stavanger, Norway
yao.zhang@uis.no
[2] Department of Mechanical and Structural Engineering and Material Science, University of Stavanger, Stavanger NO-4068, Norway

Abstract. We study the evolution of interface instabilities between Newtonian and shear-thinning fluids in a planar Hele-Shaw cell. This work builds upon a two-dimensional gap-averaged model previously developed for flow simulations involving power-law fluids in such geometries. The focus is on interfacial instability, viscous fingering dynamics, and quantifying the growth and suppression mechanisms governing perturbation evolution, specifically the growth rate of an initially perturbed fluid-fluid interface.

We conduct gap-averaged simulations using the CFD software OpenFOAM, and track the spatiotemporal evolution of an initial sinusoidal fluid-fluid interface. We compare the growth or decay rate of the initial perturbation amplitude to available analytical (linear stability) result for generalized Newtonian fluids. The results demonstrate good agreement between the 2D simulations and the theoretical linear stability analysis for Newtonian fluids, while showing notable deviations for power-law fluids, reflecting the added complexity of non-Newtonian behavior.

The influence of key parameters on the stability and dynamics of viscous fingering is systematically investigated, including rheological properties of power-law fluids such as the consistency index k and flow behavior index n, interfacial tension, and effective friction pressure gradients at the interface. For power-law fluids, interface stability is strongly influenced by the interplay between k and n. Stronger shear-thinning behavior, associated with lower n, enhances stability by increasing the effective viscosity at low shear rates, while lower k values reduce flow resistance, promoting instability and the development of viscous fingers. The effective friction pressure gradient at the interface also plays a critical role in driving instability, where a higher positive gradient promotes the development of viscous fingers, particularly under conditions of varying fluid rheology.

Keywords: Viscous Fingering, Power-Law Fluids, Hele-Shaw Cell, Interface Instability

1 Introduction

Interfacial instabilities play a crucial role in various fluid dynamics problems, particularly in multiphase flows where the stability of the interface between immiscible fluids significantly impacts flow behavior. Classical works, such as Saffman and Taylor's stability analysis of viscous fingering [1], established foundational theories demonstrating how viscosity contrasts can drive instabilities at fluid interfaces. Building on these advancements, subsequent studies have expanded the analysis to encompass diverse geometries, flow conditions, and fluid rheologies, including both Newtonian and non-Newtonian fluids [2, 3, 4, 5, 6].

These interfacial instabilities are particularly relevant in oil recovery processes, where unfavorable viscosity ratios between the displacing and displaced fluids can lead to inefficient sweep and the formation of unstable fingering patterns, reducing displacement efficiency. Salmo et al. [7] have improved the modeling of immiscible viscous fingering in porous media by incorporating fractional flow-based approaches that better capture finger evolution. Their study showed that these methods can predict water saturation distributions within fingers and adjust underlying relative permeability functions, resulting in more physically consistent representations of unstable displacements.

Recent research has further highlighted the complex interplay between fluid dynamics, flow conditions, and geometric controls in governing instability regimes. Experimental studies on pressure gradients near interfaces during viscous fingering [8] and investigations into the dynamics of instability in displacement fronts [9] underscore how fine-tuning flow geometry and conditions can influence interfacial stability.

For non-Newtonian fluids, particularly shear-thinning fluids, the instability dynamics exhibit notable differences from Newtonian fluids. Experimental studies have demonstrated that the degree of shear-thinning significantly alters the morphology of viscous fingers. Lindner et al.[10, 11] showed that for fluids with strong shear-thinning properties, the resulting fingers tend to be narrower compared to Newtonian cases, an effect attributed to the reduction in effective viscosity at high shear rates. Moreover, for weakly shear-thinning fluids, the instability can still be described using an effective Darcy's law, whereas for stronger shear-thinning effects, additional modifications are necessary to capture the observed deviations from Newtonian behavior. Varges et al.[12] further demonstrated that the displacement efficiency is highly sensitive to the rheology of the shear-thinning fluid, with lower viscosity ratios promoting more unstable interfacial patterns. Their findings highlight that the transition from an unstable to a stable displacement regime occurs at viscosity ratios that differ from those observed in Newtonian displacements, emphasizing the role of strong viscosity gradients in interfacial stability. These observations suggest that the classical Saffman-Taylor instability framework must be revisited for shear-thinning fluids, as the spatially varying viscosity field introduces additional complexity in perturbation growth and finger morphology.

To quantitatively evaluate the stability of these systems, the growth rate of perturbations at the interface serves as a critical metric. Mora and Manna [13] established a robust linear stability analysis framework that quantifies this growth rate by deriving the linear Saffman-Taylor instability for generalized Newtonian fluids in Hele-Shaw cells. Their methodology offers valuable insights into both the onset of instabilities and the conditions under which they can be mitigated or controlled. Recent studies by Lu et al. [9] expanded on this work by comparing interface growth rates for angled Hele-Shaw cells from 3D simulations to linear stability analysis results, demonstrating how parameters such as depth gradients influence instability regimes.

While 3D simulations provide detailed insights into interfacial dynamics, they are often computationally expensive, particularly when exploring a broad parameter space to observe trends and quantify the effects of key variables. To address this limitation, Zhang et al. [14] developed a 2D gap-averaged computational framework for simulating the displacement of power-law fluids in Hele-Shaw cells, offering improved computational efficiency compared to traditional 3D models. This model not only accurately replicated displacement evolution, interface morphology, and viscous fingering formation but also achieved computational efficiency over 200 times greater than traditional 3D models. The rapid computational capabilities of this 2D model enable systematic studies and direct comparisons with theoretical predictions, facilitating a deeper understanding of interfacial stability and the dynamics of viscous fingering. Preliminary findings from this work identified the effective friction pressure gradients as a critical parameter governing interface transitions, highlighting the model's potential for extensive parametric analyses and theoretical validation.

Building on this foundation, the current study utilizes the developed 2D gap-averaged model to perform a detailed analysis of interfacial instabilities during the displacement of power-law fluids in Hele-Shaw cells. The theoretical framework for growth rate predictions is adapted specifically for power-law fluids by extending the classical Saffman-Taylor model through a tailored linear stability analysis based on the work of Mora and Manna [13]. The analytical predictions are validated against results from 2D CFD simulations under controlled initial conditions with well-defined wave numbers, ensuring precise and reproducible tracking of perturbation growth.

To accurately assess instability behavior, the simulations introduce a sinusoidal perturbation at the initial interface, minimizing numerical artifacts and enabling direct comparison with theoretical predictions. The dimensionless growth rate of perturbations is systematically evaluated, providing a comprehensive analysis of how key parameters, such as rheological properties, effective friction pressure gradients, and interfacial tension, affect interface stability. The findings offer new insights into the mechanisms governing viscous fingering dynamics in power-law fluid displacement scenarios.

2 Linear stability analysis for power-law fluids

The theoretical framework proposed by Mora and Manna [13] provides a mathematical formulation for linear stability analysis for generalized

Newtonian fluids, that can be applied to a wide range of non-Newtonian fluids. In this work, we apply their general result to the specific case of power-law fluids, derives a growth rate expression that incorporates the rheological properties of shear-thinning and shear-thickening fluids. The detailed mathematical derivation is presented in the following section.

Mora and Manna [13] expressed the generalized growth rate in their Equation 35 as:

$$M = \frac{(G_2 - G_1 - \gamma k^2)k}{\sqrt{\frac{G_2}{V_2}\frac{dG_2}{dV_2}} + \sqrt{\frac{G_1}{V_1}\frac{dG_1}{dV_1}}}, \tag{1}$$

where M is the perturbation growth rate, G_i represents the unperturbed friction pressure gradient for fluid i, γ is the surface tension, and k is the wavenumber of the perturbation. V_1 and V_2 correspond to the local velocity of the displacing and displaced fluids, respectively. These velocities are related to the unperturbed friction pressure gradients via the constitutive equations governing each fluid.

For the special case of **Newtonian fluids**, this generalized Eqn. 1 simplifies to the following form (as presented in Equation 36 of [13]):

$$M = \frac{1}{\eta_2 + \eta_1} \cdot \frac{kh^2}{12} \cdot (G_2 - G_1 - \gamma k^2), \tag{2}$$

where η_1 and η_2 are the viscosities of the displacing and displaced fluids, respectively, and h is the gap width of the Hele-Shaw cell.

The friction pressure gradients G_i for Newtonian fluids can be expressed in terms of the fluid viscosities and imposed velocity U as:

$$G_i = -\frac{12\eta_i U}{h^2}. \tag{3}$$

Substituting this expression into Eqn. 2 and normalizing by U/h, the dimensionless growth rate is given by:

$$\frac{Mh}{U} = M^* = \frac{kh}{\eta_2 + \eta_1}\left[(\eta_1 - \eta_2) - \frac{\gamma k^2 h^2}{12U}\right]. \tag{4}$$

Here, the term $\frac{\gamma k^2 h^2}{U}$, associated with interfacial tension, represents capillary forces that suppress perturbation growth, particularly at higher wavenumbers.

For **power-law fluids**, the velocity $U = V_i(G_i)$ is governed by the relationship between the imposed velocity and the corresponding unperturbed friction pressure gradient G_i. This relationship simplifies to:

$$U = V_i(G_i) = \frac{(h/2)^{1+1/n_i}}{2 + 1/n_i}\frac{G_i^{1/n_i}}{k_i^{1/n_i}}, \tag{5}$$

where n_i is the flow behavior index, and k_i is the consistency index of fluid i.

The friction pressure gradient G_i can be further simplified as:

$$G_i = cV_i^{n_i}, \tag{6}$$

where c is a constant.

Substituting this into the denominator of the original growth rate Eqn. 1 gives:

$$\frac{G_i}{V_i}\frac{dG_i}{dV_i} = n_i\left(\frac{G_i}{V_i}\right)^2 = n_i\left(\frac{G_i}{U}\right)^2. \tag{7}$$

The dimensionless form of the growth rate is derived by incorporating these relationships into Eqn. 1, resulting in:

$$\frac{Mh}{U} = M^* = \frac{(1-\lambda)hk - (hk)^3/Ca}{\lambda\sqrt{n_1} + \sqrt{n_2}}, \tag{8}$$

where M^* is the dimensionless growth rate scaled by the imposed bulk velocity and the gap width of the cell from growth rate M. The parameter $\lambda \equiv G_1/G_2$ is the ratio of friction pressure gradients, and $Ca = G_2h^2/\gamma$ is the capillary number based on the friction pressure gradient of the displaced fluid.

The theoretical growth rate results calculated using Eqn. 8 are compared with the dimensionless growth rates obtained from computational simulations in Section 4.

3 Computational Method

All computational simulations in this work are conducted using the developed 2D numerical gap-averaged model. Detailed information on the model's derivation, implementation, and validation can be found in the previous publication [14]. The full implementation, including source code, case setups, and documentation, is openly available in the related GitHub repository: `https://github.com/feebsssz/heleShawFoam`.

In summary, the 2D numerical gap-averaging model is a computational framework specifically designed to simulate the displacement of power-law fluids in confined Hele-Shaw cells. The model employs a gap-averaging technique by integrating the momentum equation over the gap-wise direction of the Hele-Shaw cell, resulting in a two-dimensional formulation that preserves the essential physics of three-dimensional flow behavior.

The governing equations include gap-averaged continuity and momentum equations, where the flow field is approximated using a depth-averaged Darcy-like velocity profile. The model incorporates the non-Newtonian rheology of power-law fluids by adapting the effective viscosity term based on the local shear rate and power-law parameters. Interfacial dynamics are managed using a volume-of-fluid (VOF) approach, allowing for precise tracking of the fluid interface and accurate capture of the evolution of viscous fingering patterns.

The numerical implementation is carried out in `OpenFOAM`, with simulations executed on the University of Stavanger computing cluster utilizing multiple cores for parallel computing. Each displacement simulation runs for a duration of 20 s, with the interface evolution and perturbation growth tracked at 1 s intervals. The collected data are then fitted to an exponential growth model to quantify the perturbation growth rate. The methodology for tracking the time evolution of the fluid interface is documented in detail in the verification section of the 2D model in [14].

3.1 Geometry and Mesh configuration

The computational domain is defined as a horizontal rectangular Hele-Shaw cell with a width of 0.05 m, a narrow gap of 0.001 m, and a total length of 0.2 m. The mesh configuration employs 128 cells along the width direction, a single cell in the gap direction to maintain a two-dimensional setup, and 512 cells along the length direction.

The geometry is adapted from Lu et al. [9], whose work demonstrated robust capabilities in capturing detailed interfacial dynamics and accurately resolving viscous fingering patterns within Hele-Shaw cells for Newtonian fluid displacement. Selected cases are compared against those from Lu et al. in Sec. 4 to validate the performance of the model in predicting growth rates.

The implemented mesh configuration follows the approach established in previous work by Zhang et al. [14], where a detailed mesh convergence study was conducted to ensure both numerical accuracy and stability.

3.2 Controlled perturbation at initial interface

Previous studies have shown that viscous fingering typically develops only after initial perturbations are introduced at the fluid interface. Starting with a flat interface often makes it challenging to control instabilities, as the wavenumber and magnitude of the perturbations tend to emerge randomly and are influenced by numerical factors [14]. To address these challenges, this study introduces controlled initial perturbations with well-defined wave numbers, enabling precise quantitative comparisons with theoretical predictions from linear stability analysis.

A single sinusoidal perturbation is applied to the initial interface to ensure a controlled and reproducible onset of viscous fingering. The interface is defined by a sinusoidal wave with an amplitude of 0.004 m and a wavelength of 0.05 m, starting at a position of 0.002 m along the flow direction, corresponding to 1% of the duct length. This setup creates a single well-defined finger at the center of the duct, as shown in Fig. 1 at $t = 0$ s.

The mathematical formulation of the initial interface is expressed as $y(x) = A\sin(kx) + y_0,$, where $y(x)$ represents the interface position as a function of the horizontal coordinate x, with $A = 0.004$ m as the amplitude, $k = \frac{2\pi}{0.05} = 125.6$ m^{-1} as the wavenumber, and $y_0 = 0.002$ m as the initial vertical offset.

The initial interface configuration is implemented using the `setAlphaFieldDict` module in OpenFOAM, providing a robust and controlled starting condition for the computational simulations.

The perturbation growth is quantified by tracking the length of the viscous finger at each 1s time step throughout the simulation. At each step, the perturbation length is measured as the deviation of the finger tip at the center of the duct from the flat interface position expected in the absence of initial perturbations. The recorded perturbation lengths over time are then fitted to an exponential function to determine the growth or decay rate.

3.3 Fluid properties and Displacement configurations

More than 50 simulation cases were conducted for this study, broadly categorized into two main groups: immiscible Newtonian fluid displacement and immiscible power-law fluid displacement.

For the **Newtonian fluid displacement** cases, the simulations involve fluid pairs consisting of two immiscible Newtonian fluids under varying imposed velocities. The displaced fluid is a mineral oil with fixed properties, including a viscosity of $0.133\,\mathrm{Pa}\cdot\mathrm{s}$ and a density of $887.6\,\mathrm{kg/m^3}$. The displacing fluid is a water-based solution with a fixed density of $998\,\mathrm{kg/m^3}$, while its viscosity varies between 0.09 and $0.15\,\mathrm{Pa}\cdot\mathrm{s}$.

The interfacial tension between the two fluids is maintained at $0.0295\,\mathrm{mN/m}$ for most simulations. Additionally, to examine how surface tension influences interfacial stability and viscous fingering behavior, a dedicated set of simulations was performed with a fixed imposed velocity, U, varying the interfacial tension over a broad range from 1×10^{-10} to $0.09\,\mathrm{mN/m}$.

For the **power-law fluid displacement** cases, the simulations involve fluid pairs consisting of a power-law fluid and a Newtonian fluid. The Newtonian fluid used is the same mineral oil as in the Newtonian displacement scenarios. The power-law fluids include aqueous solutions of xanthan gum with a density of $998,\mathrm{kg/m^3}$ at varying concentrations, as well as a polyacrylamide solution with a density of $996.4,\mathrm{kg/m^3}$. Detailed power-law parameters, including the consistency index k and the flow behavior index n for both xanthan gum and polyacrylamide solutions, are reported in Table 1 of Zhang et al. [14] and complemented by fluid curve measurements of xanthan gum solutions presented in Table 2 by Amaratunga et al. [15].

In these displacement configurations, power-law fluids are used as either the displacing or the displaced fluid, paired with mineral oil under varying imposed velocities. To investigate the impact of interfacial tension, a fixed displacement configuration of oil displacing xanthan gum is employed, with the interfacial tension varied over a broad range from 1×10^{-10} to $0.04,\mathrm{mN/m}$. To assess the influence of rheological properties on interfacial stability, simulations are conducted using mineral oil as the displacing fluid with a constant interfacial tension of $0.133,\mathrm{mN/m}$, while the displaced fluid consists of xanthan gum solutions at different concentrations. These solutions offer a wide spectrum of k and n values, sourced from Amaratunga et al. [15].

The chosen fluid pairs and imposed conditions correspond to capillary numbers Ca varying from 1.071 to 0.0125, excluding extreme cases where the interfacial tension approaches zero. The ratio of friction pressure gradients $\lambda = G_1/G_2$ varies significantly across cases, ranging from 12.873 to 0.423, with the largest variations observed for different concentrations of xanthan gum solutions. These ranges capture a broad spectrum of displacement conditions, allowing for a systematic evaluation of how capillary forces and rheological effects influence interfacial stability.

4 Results and Analysis

In this section, the dimensionless growth rate of the initial perturbation, M^*, is calculated using the derived Eqn. 8 and compared with values extracted from the interface evolution tracked in the 2D CFD simulations.

4.1 Newtonian Displacement

4.1.1 Verification

To verify the accuracy of the 2D CFD simulation results, comparisons are made with the 3D direct numerical simulation (DNS) results from Lu et al.[9] and their theoretical predictions from linear stability analysis. The selected test cases 7, 8, and 9 are from the parallel Hele-Shaw geometry, with negative, zero, and positive perturbation growth rates. The fluid properties and imposed flow conditions for these cases are directly adopted from Table 1 in Lu et al.[9].

The interface evolution for the three cases is presented in Fig. 1, showing the initial interface at $t = 0$ s and the evolved interface at $t = 20$ s. When the growth rate is negative, the interface gradually flattens over time. For the zero growth rate case, the initial perturbation remains nearly stable with minimal changes in morphology and a consistent viscous finger length. Conversely, in the positive growth rate scenario, the initial perturbation grows over time, leading to an elongation of the viscous fingers.

For a more quantitative comparison, the interface was extracted at each time step, and the finger length was tracked. The method for tracking the finger length is described in Sec. 3.2. The evolution of the finger length over time is shown in Fig. 2, with comparisons to the results from Fig. 5 in Lu et al. [9].

Each figure includes two curves from Lu's work along with the results from the 2D simulation. The red curve represents the 3D model simulation results, while the black curve shows theoretical predictions from the linear growth rate analysis described in Sec. 2. The blue curve illustrates the outcomes of the 2D model simulations. As shown in the figure, the 2D simulation results for Newtonian displacement closely match both the 3D simulation results and the theoretical predictions reported in the literature, demonstrating the accuracy and reliability of the developed 2D model.

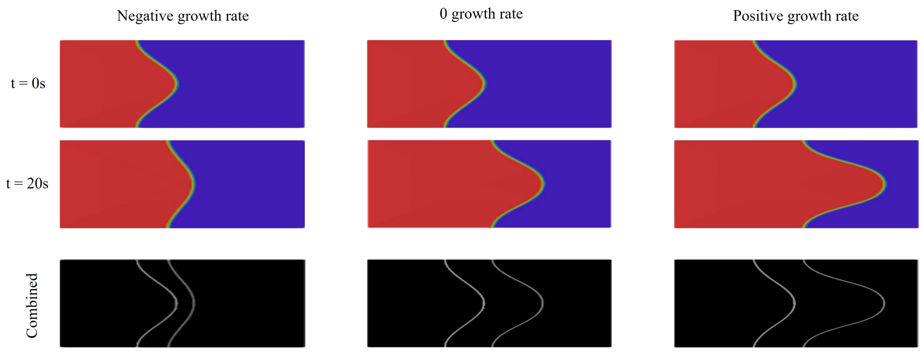

Fig. 1. Interface evolution of cases with different perturbation growth rates. The corresponding growth rate values, including comparisons with theoretical predictions, are provided in Fig. 2.

4.1.2 2D Simulations vs. Linear stability analysis

The dimensionless growth rate of the perturbation from 2D simulations, M^*, is calculated by normalizing the growth rate, M, using the imposed velocity, U, and the gap width of the Hele-Shaw cell, h, as $M^* = \frac{Mh}{U}$. This normalization provides a consistent, dimensionless metric that allows for direct comparison between the simulation results and the theoretical predictions from the linear stability analysis using Eqn. 2.

Figure 3 compares the 2D simulation results with the linear stability analysis as a cross-validation between the computational and analytical approaches. As shown in the figure, there is a strong correlation between the two methods, with the linear fit of M^* from simulations against M^* from the linear stability analysis showing a slope of 0.9072 and R^2 of 0.9998. This close agreement is consistent across a broad range of imposed velocities, fluid viscosities, and interfacial tension conditions, demonstrating the accuracy and reliability of the developed 2D model in capturing interfacial instability dynamics.

4.1.3 Influence of key parameters on perturbation growth rate

To analyze how key parameters influence the perturbation growth rate, the sensitivity of M^* to changes in interfacial tension (γ) and the effective friction pressure gradient component is systematically examined. These parameters represent to distinct physical effects represented in the growth rate equation (Eqn. 2), contributing to either the stabilization or destabilization of the fluid interface.

The theoretical predictions from linear stability analysis are included alongside the simulation results in Fig. 4. The results from simulations and linear stability analysis closely follow the same trend, effectively capturing the dependence of M^* on interfacial tension and friction pressure gradients.

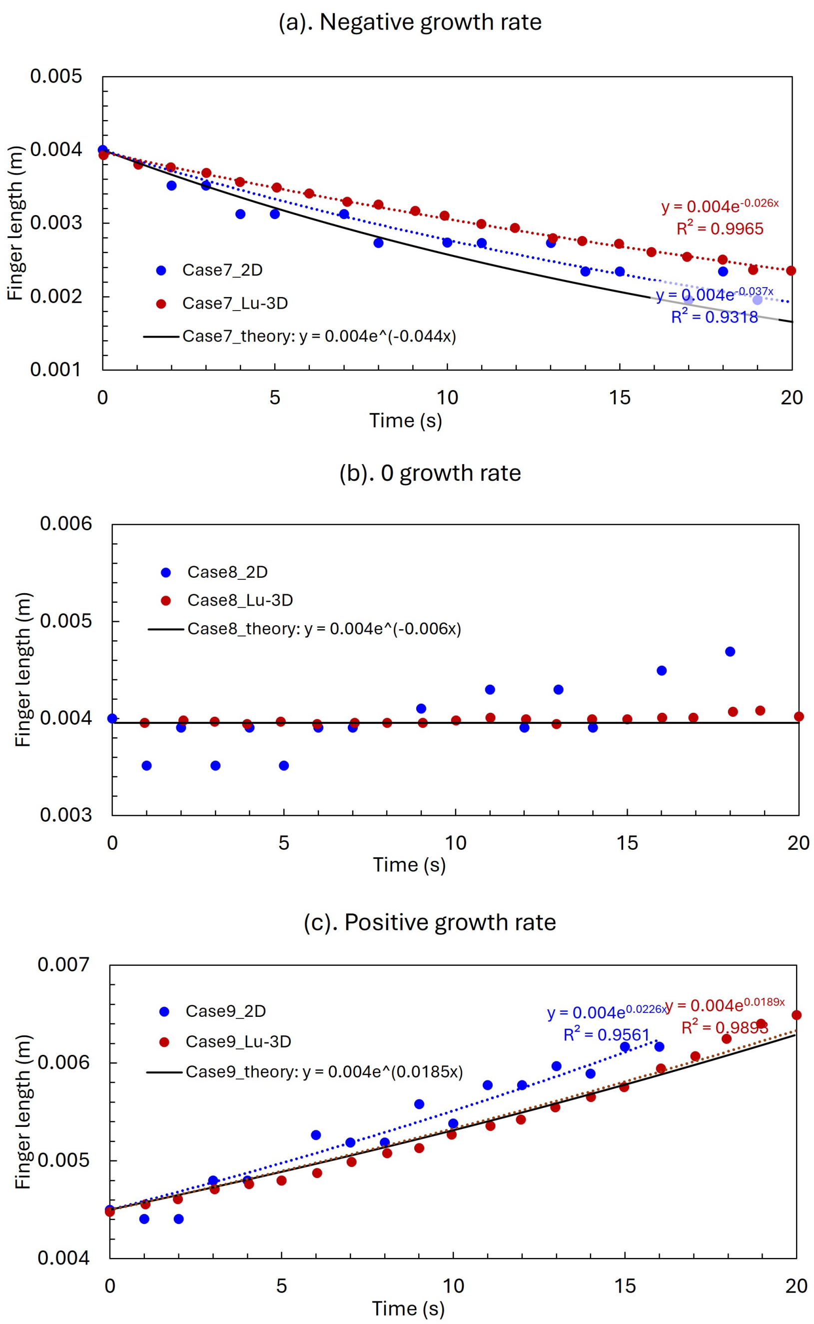

Fig. 2. Linear stability analysis verification for the finger length

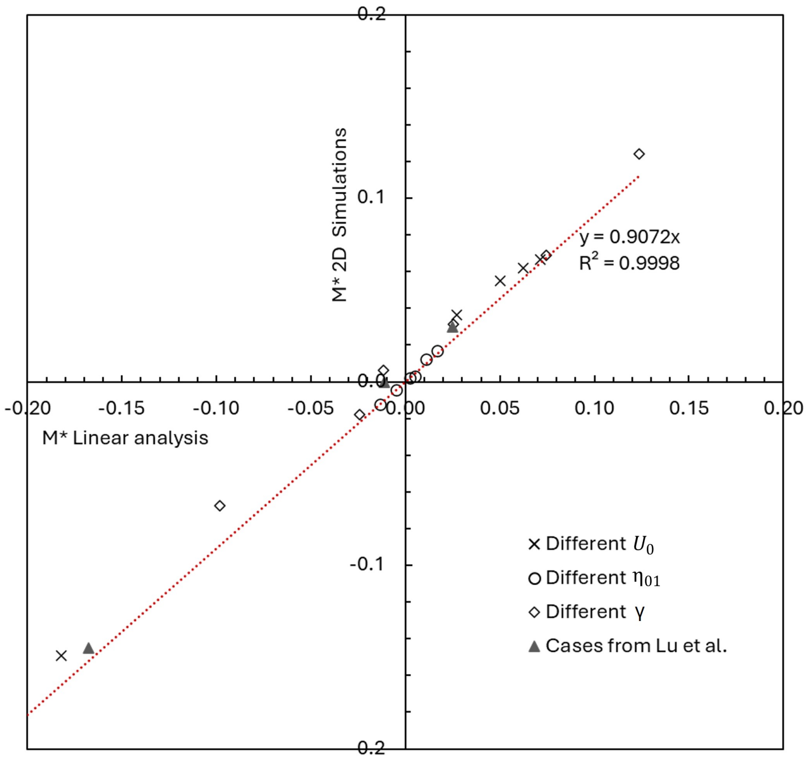

Fig. 3. Comparison of dimensionless growth rate M^* from 2D simulations and linear stability analysis for Newtonian displacement, including cases with varying imposed velocities, viscosities, and interfacial tension.

The first plot in Fig. 4 shows the influence of interfacial tension on the growth rate. Higher interfacial tension values consistently reduce M^*, demonstrating a stabilizing effect. This behavior is governed by the surface tension term γk^2 in Eqn. 2, which introduces a smoothing force at the interface, particularly effective in dampening high-wavenumber perturbations. The results emphasize the critical role of interfacial tension in counteracting instability driven by viscosity contrast and in maintaining a flatter, more stable interface.

The second plot of Fig. 4 presents the relationship between M^* and the effective friction pressure gradient component $(G_2 - G_1 - \gamma k^2)$. A strong positive correlation is observed, demonstrating that a larger positive pressure gradient enhances instability by driving the displaced fluid more aggressively through the Hele-Shaw cell. This finding is consistent with previous results reported by Zhang et al. [16], as the effective friction pressure gradient represents the net driving force for perturbation growth. When the effective friction pressure gradient is

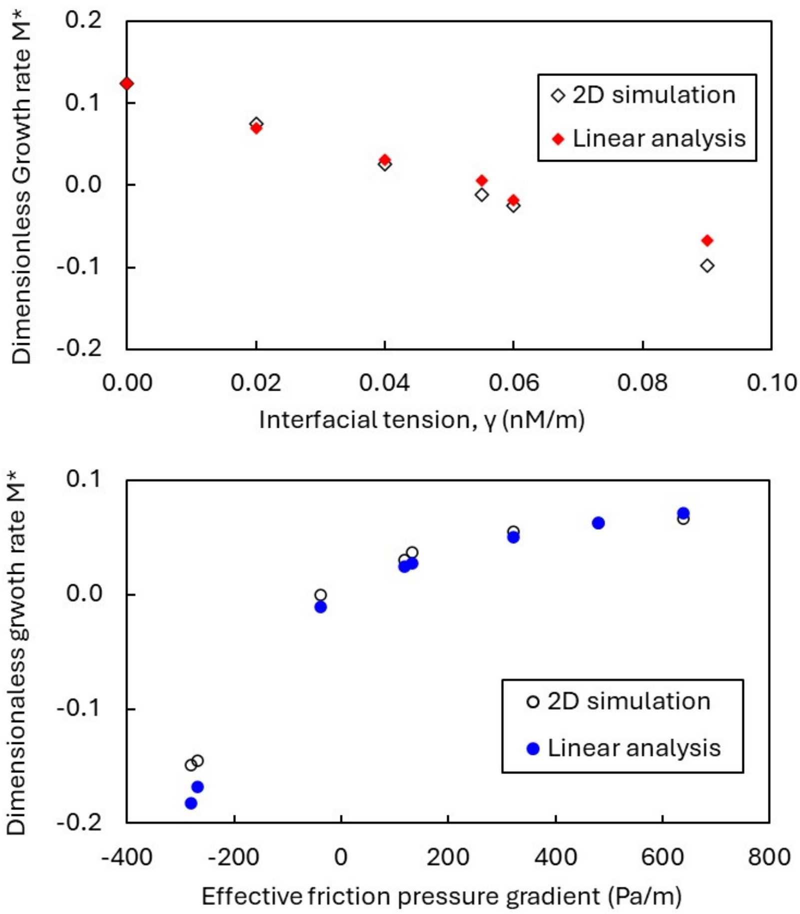

Fig. 4. Effect of interfacial tension and effective friction pressure gradient on the dimensionless growth rate M^* for Newtonian fluid.

negative or approaches zero, the system transitions toward stability, effectively suppressing the development of viscous fingers.

4.2 Power-Law Fluid Displacement

For power-law fluids, a similar approach is applied to evaluate the dimensionless growth rate, M^*. The growth rate from 2D simulations is extracted using the same methodology as for Newtonian fluids, while the theoretical growth rate for power-law fluids is calculated using Eqn. 8 derived in Section 2.

4.2.1 2D simulations vs. Linear stability analysis

The comparison between the 2D simulation results and the linear stability analysis is shown in Fig. 5.

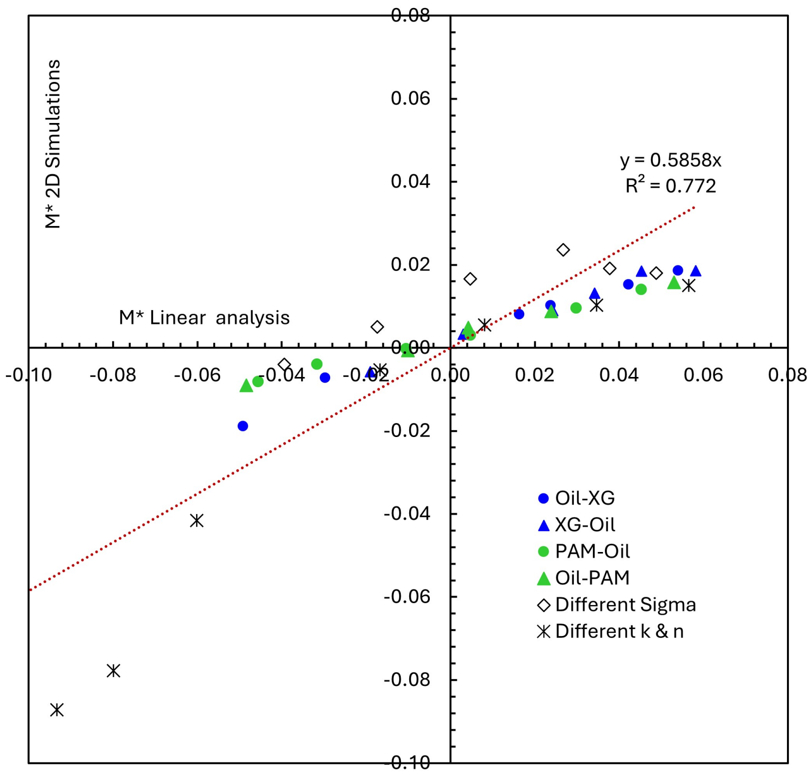

Fig. 5. Comparison of dimensionless growth rate M^* from 2D simulations and linear stability analysis for power-law fluids, including various fluid pairs and conditions with different interfacial tensions and power-law parameters k and n.

Unlike the Newtonian fluid cases, which demonstrated near-perfect alignment between 2D simulations and linear stability analysis, the power-law fluid results exhibit a more scattered distribution around the 1-to-1 line. While the overall trend remains linear, significant deviations are observed, particularly in scenarios with variable interfacial tension and differing power-law parameters k and n.

This scatter indicates that the linear stability analysis for power-law fluids may not fully capture the complexities observed in the 2D simulations. The discrepancies are particularly pronounced under conditions of high non-linearity, such as extreme values of the flow behavior index n or cases with substantial variations in interfacial tension. These findings suggest that while the linear theory provides a useful first-order approximation, the displacement of power-law fluids in Hele-Shaw cells involves additional dynamics. These dynamics are likely influenced by non-linear effects and complex fluid rheology, which are not fully addressed by the current linear stability model.

Furthermore, a known limitation in the 2D gap-averaged model could contribute to the underestimation of M^* in power-law fluid cases. As noted in [14], the evaluation of $\nabla_0 \cdot \tau$ in Eq. (9) does not fully account for cross-gap shear when computing τ, leading to an effective viscosity that is higher than expected. This may explain the reduced perturbation growth rate observed in the 2D simulations, as shown in Fig. 5. Since this issue primarily affects shear-dependent viscosity calculations, it does not impact Newtonian fluids, resulting in a better agreement between the 2D model and theoretical predictions for Newtonian cases, as shown in Fig. 3. Addressing this limitation would require a more refined treatment of the cross-gap shear effect to improve the accuracy of perturbation growth rate predictions for power-law fluids.

4.2.2 Influence of key parameters on perturbation growth rate

The dimensionless growth rate of perturbations, M^*, for power-law fluids is governed by a complex interplay of parameters, as defined in Eqn. 8. The key influencing factors include the ratio of friction pressure gradients λ, the interfacial tension γ, and the rheological properties represented by the flow behavior index n and the consistency index k. The impact of these parameters on M^* is systematically examined.

The top plot in Fig. 6 shows the sensitivity of the growth rate to changes in the ratio of friction pressure gradients, expressed as $\frac{1}{\lambda} = \frac{G_2}{G_1}$. The results show that when $\frac{1}{\lambda}$ is above unity, M^* is positive, indicating that the perturbation grows over time. Conversely, when this ratio is below unity, M^* is negative, suggesting that the interface transitions to a stable regime where perturbations decay. This behavior aligns with the findings of Zhang et al. [14], where the transition from a flat interface to viscous fingering occurred when the ratio of friction pressure gradients approached unity ($\lambda \approx 1$). Note that both the theoretical predictions and 2D simulation results exhibit a similar logarithmic dependence of M^* on $\frac{1}{\lambda}$, consistent with the trend observed for Newtonian fluids in Fig. 4, where the theoretical growth rate also follows a logarithmic relationship with the effective friction pressure gradient.

The second plot in Fig. 6 shows the effect of interfacial tension on the growth rate. Consistent with the behavior observed in Newtonian fluids, higher interfacial tension values lead to a reduction in M^*, promoting interface stability. This stabilizing influence stems from the surface tension term $\frac{(hk)^3}{Ca}$ in Eqn. 8, which increases with higher γ and dampens the growth of small-scale perturbations. The results confirm that surface tension acts as a smoothing force, particularly effective in suppressing high-wavenumber perturbations and enhancing interface stability. Comparison between theoretical predictions and 2D simulations shows that while M^* decreases approximately linearly with increasing interfacial tension in the linear analysis, the 2D simulation results exhibit a weaker dependence at lower interfacial tension values and overpredict the growth rate at higher interfacial tensions.

The third plot in Fig. 6 examines how the flow behavior index n influences the growth rate. Both the theoretical predictions and 2D simulation results follow a similar linear trend, showing a steady increase in M^* with n. The results indicate that higher values of n generally lead to increased perturbation growth rates, while lower n values enhance stability. However, the discrepancy between theory and simulation is more pronounced at lower n values, where the 2D simulations predict lower growth rates compared to theoretical expectations. As n increases and the fluid behavior approaches Newtonian-like characteristics, the difference between the theoretical and simulated results diminishes, leading to better agreement. One possible reason for this discrepancy is that the 2D gap-averaged model does not fully account for cross-gap shearing effects, resulting in an overestimation of viscosity in the shear-thinning regime.

The bottom heatmap in Fig. 6 provides insights into the combined effects of the consistency index k and the flow behavior index n on M^*. The results show a clear trend where higher k and lower n values contribute to increased growth rates. The combination of high k and low n leads to the highest growth rates, as the high baseline viscosity increases viscosity contrast, while the strong shear-thinning behavior enhances interface deformation under stress. This dual effect promotes instability development, making the interface more susceptible to viscous fingering and perturbation growth during fluid displacement processes.

5 Discussion

In this work, the analysis of perturbation growth rates in both Newtonian and power-law fluid systems within Hele-Shaw cells provides valuable insights into the parameters that influence viscous fingering dynamics. The 2D computational simulations are compared with the linear stability analysis to evaluate accuracy and reveal key stability mechanisms.

5.1 Newtonian vs. Power-law fluid

The perturbation growth rate, M^*, for both Newtonian and power-law fluid systems is primarily governed by three critical parameters: interfacial tension γ, the viscosity ratio (or its equivalent rheological parameters for power-law fluids), and the effective friction pressure gradient. These parameters influence whether the interface remains stable or transitions into a viscous fingering regime.

For **Newtonian fluids**, higher interfacial tension consistently promotes stability by suppressing small-scale perturbations through the γk^2 term in the growth rate equation. This effect smooths the interface and dampens high-frequency disturbances, reducing the likelihood of viscous fingering. The viscosity contrast between the displacing and displaced fluids also plays a critical role; a larger viscosity contrast, where the displacing fluid has a significantly lower viscosity, destabilizes the interface by increasing M^* and promoting viscous finger growth. Additionally, the effective friction pressure gradient is a key factor influencing the growth rate. Positive friction pressure gradients drive instability by amplifying perturbations, while negative or balanced gradients contribute to a stable interface.

For **power-law fluids**, similar trends are observed, but the behavior is further modulated by the fluid's rheological properties, specifically the consistency index k and the flow behavior index n. The interplay between k and n introduces complexity not present in Newtonian fluids. Lower n values, indicating stronger shear-thinning behavior, enhance stability by increasing the effective viscosity at lower shear rates, dampening perturbation growth. Conversely, lower k values, which indicate lower effective viscosity, promote instability by reducing flow resistance and facilitating the development of viscous fingers. The combined effect of k and n is particularly evident in the heatmap analysis, demonstrating how a balance between these parameters determines whether the interface remains stable or undergoes fingering. Similar to Newtonian cases, higher interfacial tension contributes to stability by reducing M^*. The effective friction pressure gradient ratio also controls whether perturbations grow or decay, directly impacting whether the interface remains stable or transitions to a fingering pattern.

Overall, while both fluid types share foundational stability mechanisms, such as the stabilizing influence of interfacial tension and the critical role of friction pressure gradients, the rheological complexity of power-law fluids introduces additional control through the k and n parameters. Unlike Newtonian fluids with constant viscosity, power-law fluids dynamically adapt their effective viscosity to flow conditions. The flow behavior index n introduces shear-thinning or shear-thickening effects, offering a more complex mechanism that can either dampen or enhance instability depending on the fluid's response to shear.

5.2 2D Model vs. Linear stability analysis

While the 2D numerical model aligns well with the linear stability analysis for Newtonian fluids, discrepancies are more pronounced in power-law fluid cases. The linear stability analysis captures the general trend of stability versus instability, but deviations arise in cases involving strong shear-thinning effects or significant variations in interfacial tension. The scatter observed in the comparison plot in Fig. 5 suggests that additional factors influence the perturbation growth rate beyond what is accounted for in the theoretical model.

One potential explanation for these discrepancies is the known limitation in the 2D gap-averaged model when computing the shear stress divergence, $\nabla_0 \cdot \tau$, as discussed in [14]. In power-law fluids, this calculation does not fully account for cross-gap shear, leading to an overestimation of effective viscosity and, consequently, a reduced perturbation growth rate in the 2D simulations. This issue is absent in Newtonian fluids, where viscosity remains constant, allowing for a strong agreement between the 2D model and the linear stability analysis in that limit.

Thus, while the linear stability model does not incorporate all non-linear effects present in the simulations, the observed discrepancies in power-law cases are likely influenced by limitations in the 2D model rather than inherent inaccuracies in the theoretical framework. Addressing these limitations in the 2D model, particularly in how it handles shear-dependent viscosity calculations, would provide a clearer assessment of the predictive accuracy of the linear stability analysis in non-Newtonian fluid systems.

References

[1] P. G. Saffman and G. I. Taylor. "The penetration of a fluid into a porous medium or Hele-Shaw cell containing a more viscous liquid". In: *Proc. R. Soc. Lond. A* 245 (1958), pp. 312–329. DOI: 10.1098/rspa.1958.0085.

[2] T. T. Al-Housseiny, P. A. Tsai, and H. A. Stone. "Control of interfacial instabilities using flow geometry". In: *Nature Phys* 8 (2012), pp. 747–750. DOI: 10.1038/nphys2396.

[3] T. T. Al-Housseiny and H. A. Stone. "Controlling viscous fingering in tapered Hele-Shaw cells". In: *Phys. Fluids* 25 (2013), p. 092102. DOI: 10.1063/1.4819317.

[4] Pedro HA Anjos, Eduardo O Dias, and José A Miranda. "Radial fingering under arbitrary viscosity and density ratios". In: *Physical Review Fluids* 2.8 (2017), p. 084004.

[5] Grégoire Bongrand and Peichun Amy Tsai. "Manipulation of viscous fingering in a radially tapered cell geometry". In: *Physical Review E* 97.6 (2018), p. 061101.

[6] Eduardo O Dias et al. "Minimization of viscous fluid fingering: a variational scheme for optimal flow rates". In: *Physical review letters* 109.14 (2012), p. 144502.

[7] Iselin Cecilie Salmo et al. "Immiscible viscous fingering: modelling unstable water–oil displacement experiments in porous media". In: *Transport in Porous Media* 145.2 (2022), pp. 291–322.

[8] Savannah D Gowen, Thomas E Videbæk, and Sidney R Nagel. "Measurement of pressure gradients near the interface in the viscous fingering instability". In: *Physical Review Fluids* 9.5 (2024), p. 053902.

[9] Daihui Lu, Federico Municchi, and Ivan C Christov. "Computational analysis of interfacial dynamics in angled Hele-Shaw cells: instability regimes". In: *Transport in Porous Media* 131.3 (2020), pp. 907–934.

[10] Anke Lindner, Daniel Bonn, and Jacques Meunier. "Viscous fingering in a shear-thinning fluid". In: *Physics of Fluids* 12.2 (2000), pp. 256–261.

[11] Anke Lindner et al. "Viscous fingering in non-Newtonian fluids". In: *Journal of Fluid Mechanics* 469 (2002), pp. 237–256.

[12] PR Varges et al. "Immiscible liquid-liquid displacement flows in a Hele-Shaw cell including shear thinning effects". In: *Physics of Fluids* 32.1 (2020).

[13] S. Mora and M. Manna. "Saffman-Taylor instability for generalized Newtonian fluids". In: *Phys. Rev. E* 80 (1 July 2009), p. 016308. DOI: 10 . 1103 / PhysRevE . 80 . 016308. URL: https://link.aps.org/doi/10.1103/PhysRevE.80.016308.

[14] Yao Zhang et al. "Numerical modeling of fluid displacement in Hele-Shaw cells: a gap-averaged approach for power-law and Newtonian fluids". In: *Rheologica Acta* (2025), pp. 1–16.

[15] Maduranga Amaratunga et al. "Predicting rheological properties of water-based polymer mixtures from their component properties – Poly-Anionic Cellulose and Xanthan gum". In: *ANNUAL TRANSACTIONS OF THE NORDIC RHEOLOGY SOCIETY, VOL. 26.* 2018.

[16] Yao Zhang, Andrianifaliana H Rabenjafimanantsoa, and Hans Joakim Skadsem. "Interfacial Dynamics of Miscible Displacement of Shear-Thinning Fluid in a Vertical Channel". In: *Fluids* 8.2 (2023), p. 35.

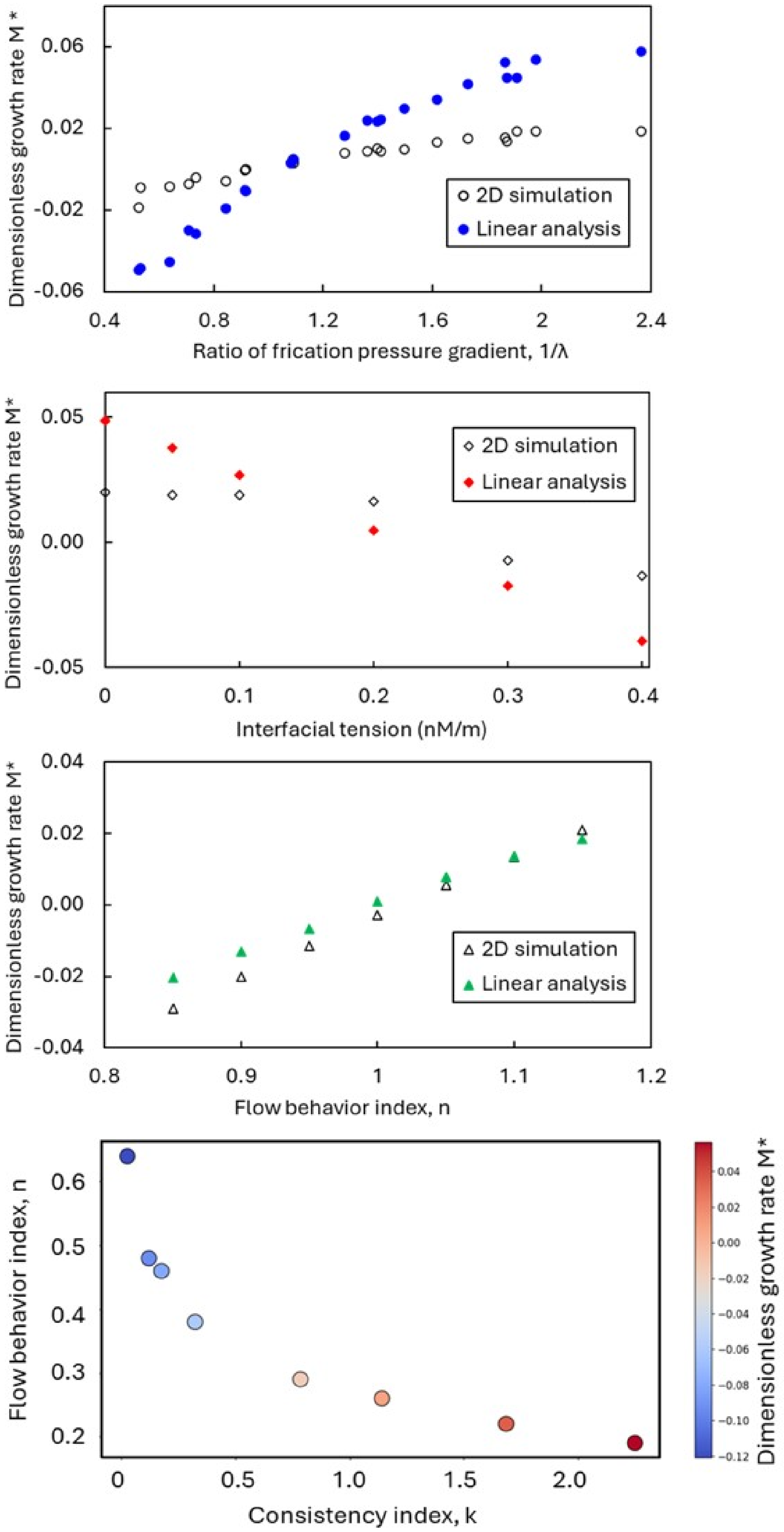

Fig. 6. Effect of key parameters on the dimensionless growth rate M^* for power-law fluids: (Top) Ratio of friction pressure gradients $\frac{1}{\lambda}$, (Second) Interfacial tension, (Third) Flow behavior index n, (Bottom) Combined influence of consistency index k and flow behavior index n.